Nanosecond Thermometry with Josephson Junctions

M. Zgirski,[1,][*] M. Foltyn,[1] A. Savin,[2] K. Norowski,[1] M. Meschke,[2] and J. Pekola[2]

[1]*Institute of Physics, Polish Academy of Sciences, Aleja Lotnikow 32/46, 02-668 Warsaw, Poland*

[2]*Low Temperature Laboratory, Department of Applied Physics, Aalto University School of Science, P.O. Box 13500, FI-00076 Aalto, Finland*

We demonstrate a new paradigm in nanoscale thermometry exploiting well-known switching measurements of a superconducting weak link. Such a weak link probed with nanosecond current pulses serves as a temperature-sensing element and, because of the fast inherent dynamics, is capable of delivering unprecedented temporal resolution. We use the thermometer to measure the dynamic temperature of electrons in a long superconducting wire relaxing to the bath temperature after application of a heating pulse, involving evaluation of the retrapping time. Our measurement delivers resolution better than 10 ns, with potential for further improvement. It extends the temporal resolution of existing experiments and introduces new possibilities for investigating thermodynamics at the nanoscale.

I. INTRODUCTION

Investigations of thermal processes in mesoscopic systems demand fast thermometry that can be easily integrated with a structure [1–3]. With reduction of the volume of a thermodynamic system, its thermal inertia rapidly vanishes, leaving often a very-short time interval for observation of a transient from which all important thermodynamic quantities can be derived. Static methods use normal-metal–insulator–superconductor tunnel junctions (NIS) [4], superconducting-quantum-interference-device (SQUID) noise thermometry [5], or quantum dots [6] to explore hot-electron effects [7], quantization of heat conductance [8–10], build Maxwell's demons [11] and microcoolers [12]. Some dynamic thermal properties were measured in steady states; for example, the relaxation time of excess electron energy to a phonon bath τ_{ep} can be obtained by measurement of electron-phonon thermal conductance G_{ep} and under the assumption of the usual linear temperature dependence for the electronic heat capacity [7]. However, to obtain a complete understanding of thermodynamics at the nanoscale, one needs obviously to have a thermometer operating at timescales much shorter than thermal relaxation times [1,3,13]. The typical thermal relaxation time τ of a nanoisland is the ratio of its heat capacity C to its thermal conductance G, providing a path to a thermal reservoir for excess energy. If such an island is used as a sensing element of a bolometer (e.g., absorbing single photons), to increase device sensitivity, it is highly desirable to reduce its heat capacity to maximize

the temperature rise on photon absorption ($\Delta T = h\nu/C$) and reduce thermal conductance to the reservoir. However, such optimization may lead to reduction of the relaxation time of the nanoisland, calling for the application of even-faster thermometers. Fast thermometry would also lend strong support to the development of cryoelectronics and quantum-computing devices, making it possible to control the temperature of different components of the devices and monitor their thermal coupling to the environment.

One approach to boost the temporal resolution of a thermometer is to embed a temperature sensor in a microwave or rf resonator [1,3,13]. A change in the magnitude and phase of the transmitted or reflected signal provides information about the thermal dynamics of the system. The method circumvents the problem of unavoidable stray-cabling capacitance, offering a typical bandwidth of 10 MHz. The need to use a resonator increases the sensor complexity and inhibits a higher level of integration (microwave on-chip resonators are millimeter-sized structures). Another interesting scheme to gain access to dynamic properties of nanocircuits, that recently yielded energy-relaxation rates in metallic wires, is measurement of noise modulation in response to ac excitation with application of a vector network analyzer [14].

In an effort to explore thermal processes at significantly faster rates, we develop a completely different strategy: we use a hysteretic superconducting weak link probed with fast current pulses for its switching threshold as a temperature-sensing element. Our thermometer is capable of measuring temperature transients with unprecedented temporal resolution, being inherently limited only by the plasma frequency of the Josephson junction (JJ),

---

with response in the picosecond range. Moreover, it also exhibits other valuable characteristics: (i) it is, a very-small all-solid-state-based thermometer; (ii) it is very simple to fabricate (e.g., the Dayem nanobridge is just a piece of a nanowire interrupting a thicker wire); (iii) it can be easily integrated with different nanostructures, providing high spatial resolution for the temperature read-out; and (iv) it requires a much-simpler hardware configuration compared with existing rf techniques. The ease of integration, true nanometer size, and simplicity make our thermometer a good choice for investigating thermodynamics of nanocircuits and offers, to a limited extent, a diagnostic tool for developing time-resolved bolometers—detectors of electromagnetic radiation, especially in the far-infrared and terahertz band—for health [15], security [16] and astronomical [17] applications. Although our protocol addresses only perfectly repeatable thermal processes, which can be restarted with the same initial conditions many times, the switching thermometry, as described below, can prove to be very attractive in many physical experiments; for example, in determination of heat capacity and thermal conductivity, in studying mechanisms of heat exchange in nanostructures, or even in experiments detecting single photons [18–20], provided that one can launch them on demand synchronized to the pulses probing the JJ.

Below we describe our approach to fast thermometry at the nanoscale. First we show how the switching feature of any superconducting weak link (i.e., its transition from the superconducting to the normal state) can be used to derive the weak-link temperature. We validate the probing protocol introduced by studying the dynamic temperature of our model system (aluminum superconducting nanowire) with true nanosecond resolution, and compare our measurement with the prediction of the heat-flow equation. Subsequently, before a summary, we outline the powerful perspectives for future studies that our method brings.

II. JOSEPHSON JUNCTION AS A TEMPERATURE-SENSITIVE SWITCH

JJs are sometimes referred to as "switches" for their ability to carry supercurrent only to a certain level, and above this level they switch to a finite voltage state (Fig. 1). The method for the switching current measurement is known [21–24]. A rectangular current pulse is applied to the junction, and the response of the junction is measured: it switches or remains in the superconducting state. The switching process exhibits stochastic character, for it involves thermal or quantum fluctuations driving the JJ out of its metastable state [25,26]. Sending a pulse train allows one to determine the switching probability P corresponding to a given pulse amplitude. Repeating the same experiment for different current amplitudes gives what is called an "S curve": the current amplitude dependence
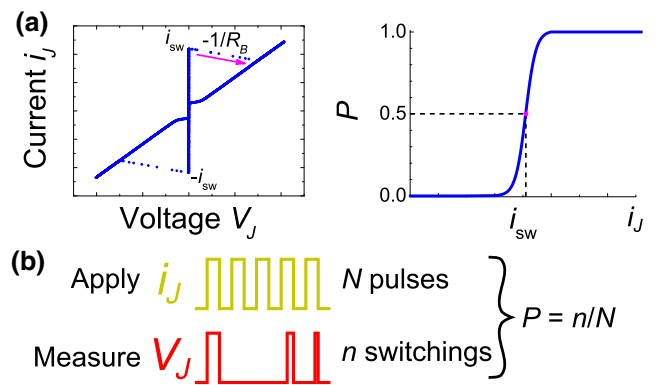

FIG. 1. Switching current measurement. (a) I-V characteristics of a JJ biased through a bias resistor with resistance R_B (see Fig. 4). The JJ supports supercurrent only to a certain level. When the threshold value i_{sw} is crossed, a finite voltage develops across the JJ. The dots, revealing a bias line with slope $-1/R_B$, are measurement artifacts related to the finite response of room-temperature electronics. In reality the switching process is instantaneous. (b) An estimator for the switching probability P at a given current amplitude i_J is measured with a train of N pulses. (c) An S curve: $P(i_J)$ dependence.

of the switching probability (Fig. 1). Switching experiments on JJs have shed some light on the nature of Andreev bound states in superconducting point contacts [21,22], have been used for magnetization measurements with nanoSQUIDs [27], and have been statistically studied, proving to be useful for generating random numbers [23].

The key observation in the current context is the dependency of the switching-current threshold on temperature (Fig. 2) [28], a feature required for a temperature sensor. The JJ thermometer is calibrated by our measuring its switching current corresponding to $P = 0.5$ against the bath temperature T_0 (see Appendix A). The calibration curve $i_{sw}(T)$ can be understood within the framework treating the superconducting weak link as a set of transmission channels [Eqs. (15) and (16) in [29]]. In the regime of diffusive transport (mean free path much less than the length of the bridge), which is the case for our nanobridge, transmissions of the channels become small ($\tau_i \ll 1$) and the general expression for the Josephson current reduces to the Ambegaokar-Baratoff result, derived first for tunnel junctions [30]:

$$I_C(T) = \left[\frac{\pi \Delta(T)}{2eR_T}\right] \tanh \left[\frac{\Delta(T)}{2k_B T}\right], \qquad (1)$$

where $\Delta(T)$ is the temperature-dependent superconducting gap and R_T is the normal-state resistance of the junction. The dependence is in agreement with our calibration curve yielding a proper order of magnitude resistance for the bridge (Fig. 2). The thermometer remains sensitive down
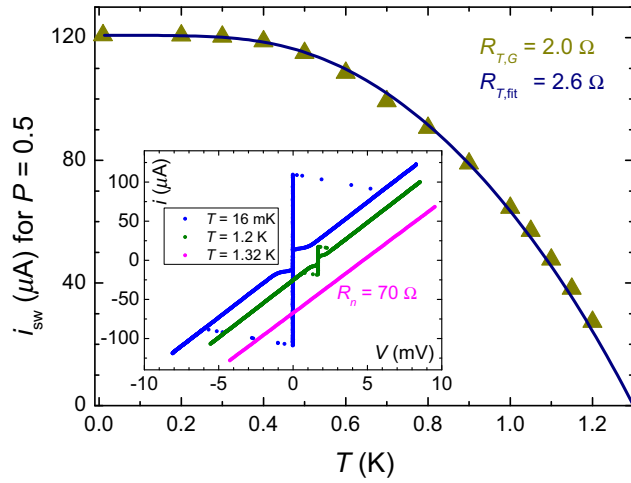
FIG. 2. Calibration curve. Temperature dependence of the switching current for the superconducting weak link studied in this work. The solid line represents the Ambegaokar-Baratoff prediction (Eq. 1) with $R_{T,\text{fit}}$ being the only adjustable parameter. $R_{T,G}$ is the calculated weak-link resistance assuming $\rho = 2 \times 10^{-8}\,\Omega$, length 180 nm, width 60 nm, and thickness 30 nm. The inset shows I-V curves obtained at three temperatures: 16.5 mK, 1.2 K, and 1.32 K (from left to right, offset horizontally).

to 250 mK. It is important to stress that this temperature is not the limit for the method presented in general (see Sec. VII).

To bring in the temporal resolution of the thermometer, we use a *pump*-and-*probe* idea, somewhat familiar from

laser physics. This is the key ingredient for our approach: a nanostructure in thermal contact with the JJ is heated with a pump pulse and then, say, several dozen nanoseconds later, the JJ is tested with a probe pulse (Fig. 3). The probe-pulse amplitude is adjusted with a bisection algorithm to yield switching probability $P = 0.5$. The delay between the pump pulse and the probe pulse can be controlled with accuracy of a single nanosecond, providing unprecedented resolution. It is worth highlighting a probe-and-hold feature of the JJ: the JJ reaches terahertz-response bandwidth, but, due to hysteresis (the retrapping current at which the JJ returns to the superconducting state is much lower than the switching current) and with a properly tailored probe pulse (Fig. 3), read-out may be implemented with low-frequency lines.

III. MODEL SYSTEM FOR TESTING THE PROPOSED THERMOMETRY

The suggested thermometry scheme can be realized based on different types of JJs, such as tunneling JJs (a very-thin oxide layer sandwiched between two superconducting electrodes), proximity JJs (a piece of normal metal interrupting a superconductor), or superconducting bridges (e.g., Dayem nanobridges) [31]. In the current work an aluminum Dayem nanobridge is used to demonstrate the applicability and reliability of the proposed thermometry and highlight its superior temporal sensitivity. The device is presented in Fig. 4. It consists of a narrow superconducting bridge placed in the middle of superconducting
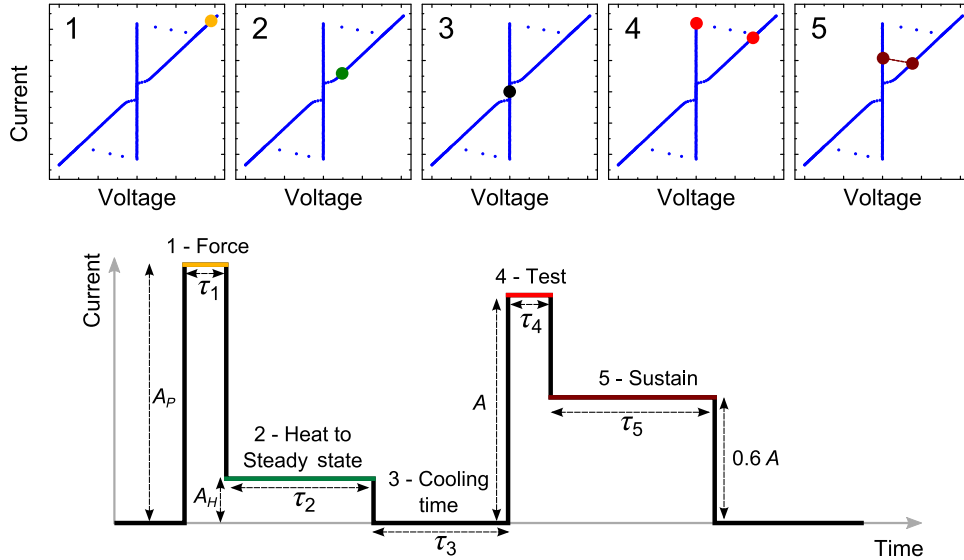

FIG. 3. The principle of the pump-and-probe experiment. By applying a current pulse larger than the switching threshold, we force the junction to go to the normal state (1). Then we bring the junction and its surroundings to a thermal steady state (2). The probe sequence (4, 5) is delayed by time τ_3 (3) with respect to the pump sequence (1, 2), and its testing part (4), if tuned to obtain switching probability $P = 0.5$, measures the instantaneous temperature in the middle of the wire. The sustain part of the probe sequence (5) allows read-out with slow room-temperature electronics: if the junction switches, a finite voltage is detected, otherwise no voltage builds up on the probing wires. A_P, A_H, and A denote current amplitudes for different parts of the pump and probe pulses.
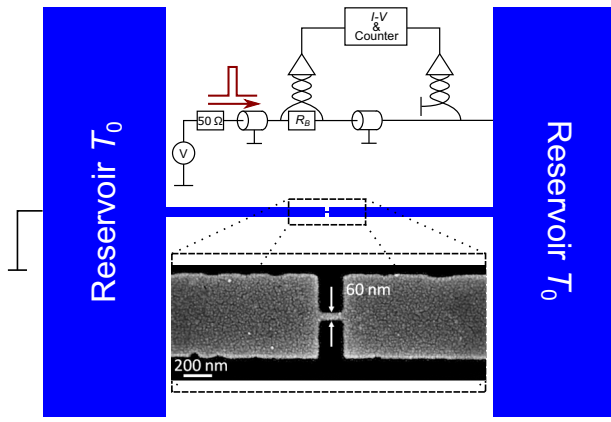
FIG. 4. Nanostructure and measurement setup used to benchmark the proposed thermometry. A wire of length 75 μm is interrupted in the middle with a Dayem nanobridge. The width of the wire is 600 nm and its thickness is 30 nm. Two voltage amplifiers depicted by triangles measure the current i_J flowing into the nanobridge and the voltage V_J across it.

wire anchored at both ends to large-area contact pads serving as energy reservoirs. Such a structure is easily obtained on a silicon substrate with conventional one-step electron-beam lithography and, what is important for benchmarking, its thermal dynamics is easy to simulate as the thermal properties of aluminum are well known. The device is placed in a dilution refrigerator with a base temperature of 10 mK. First we measure the dependence of its switching current on temperature $i_{sw}(T)$ at well-defined bath temperatures determined with a conventional calibrated RuO$_x$ thermometer (Fig. 2). Then, with application of a pump and probe pulse train, we perform switching-current-relaxation measurements of the junction after it switched first to a normal state, was then brought to a steady state, and was finally left to cool down. For each delay between the pump pulse and the probe pulse, we find the switching-current amplitude corresponding to switching probability $P = 0.5$. We send a train of 10 000 pump and probe pulses to measure each point. A period of 100 μs ensures complete thermal relaxation after each pump and probe pulse.

IV. NANOSECOND-RESOLUTION THERMOMETRY

The measured relaxation of the switching current [Fig. 5(a)] is converted into a temporal profile of the dynamic temperature [Fig. 5(b)] with the aid of the $i_{sw}(T)$ calibration curve (Fig. 2) [32]. The logarithmic scale reveals the nanosecond-resolution capability of the thermometer. Each point in the profile has limited precision both in time and in temperature. As shown conservatively in Appendix B, the temporal uncertainty is not worse than the duration of the testing pulse (i.e., about 10 ns

in this study). The temperature precision is limited both by the accuracy of the bisection algorithm and by the probabilistic nature of the measurement. The bisection algorithm iteratively finds the switching current corresponding to probability $P = P_{goal} \pm \Delta P_{acc}$ (the search is stopped when measurement yields the probability from the specified interval). In the current experiment $P_{goal} = 0.5$ and $\Delta P_{acc} = 0.02$. The finite number of pulses applied to measure the probability accounts, in addition, for statistical broadening of the measurement; that is, $\Delta P_s = [P_{goal}(1 - P_{goal})N]^{1/2}$ [Fig. 5(d)]. Thus the total probability uncertainty for $N = 10\,000$ pulses is $\Delta P = \Delta P_{acc} + \Delta P_s = 0.025$. This translates into the following uncertainty in the current corresponding to switching probability $P_{goal} = 0.5$: $\Delta I_{sw} = (\partial P / \partial I_{sw})^{-1} \Delta P$, with the derivative being the slope of the S curve at $P = 0.5$ [Fig. 5(c)]. For the final determination of the dynamic temperature, one needs to consider this uncertainty twice: for the calibration curve $I_{sw}(T)$ and for the actual I_{sw}-versus-time profile. The corresponding precision of the temperature determination is $\Delta T = 2\Delta I_{sw}|(\partial I_{sw}/\partial T)^{-1}| = 0.05(\partial P/\partial I_{sw})^{-1})|(\partial I_{sw}/\partial T)^{-1}|$. For $N = 10\,000$, the temperature uncertainty is presented in Fig. 5(b), with bigger uncertainties observed at lower temperatures reflecting suppression of the sensitivity $\partial I_{sw}/\partial T$ (see Fig. 2). For $N = 100$, the measuring time is 100 times shorter but the uncertainty grows by a factor of 10.

We can monitor the temperature of the link immediately after it reenters (retraps) the superconducting state, about 20 ns after the heating current is switched off [Fig. 5(b)]. It is the upper limit for the retrapping time of the superconducting nanowire. It can be viewed as the dead time of our measurement, but not of the thermometer in general: we use the same weak link both for heating the wire to an elevated temperature and for sensing the dynamic temperature during relaxation. For heating we need to transfer the weak link to the normal state; for sensing it must be in the superconducting state. Transition between these two states requires several dozen nanoseconds. It is possible to make these two functionalities independent by introduction of a separate heater and elimination of the dead time in experiments.

The bridge can be tested with current pulses of different duration τ_4 [Fig. 5(a)]. For measurements performed at constant temperature (with no relaxation) we expect to measure larger switching currents for shorter pulses. This directly follows from the relation $P = 1 - \exp[-\Gamma(i_b)\tau_4]$ (switching rate Γ depends on the biasing current i_b). However, if switching is measured during fast thermal relaxation, we observe the same switching current independent of the duration of the testing pulse: for short-enough cooling times, the curves of the switching current versus cooling time are superimposed on each other [Fig. 5(a)]. This is a signature of very-rapid decrease of the temperature of the bridge. If in this case the weak link does not
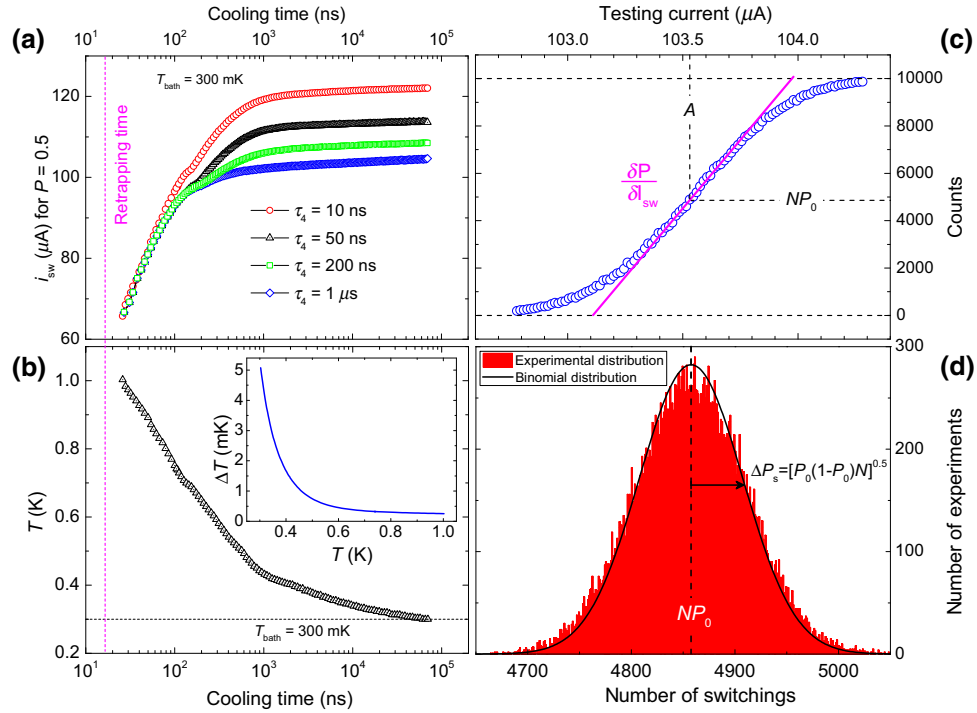
FIG. 5. Nanowire thermal dynamics. (a) Relaxation of the switching current measured with different testing pulses. The pump and probe pulses used in the experiment are shown in the Fig. 3. The timing is as follows: $\tau_1 = 100$ ns, $\tau_2 = 5$ μs, τ_3 cooling time, τ_4 (displayed in the figure), $\tau_5 = 3$ μs. (b) Electron temperature (triangles) and its calculated uncertainty $\Delta T(T)$ (inset). The temperature is inferred for the $\tau_4 = 10$ ns curve from (a). A graphical conversion is presented in Supplemental Material [32]. (c) An S curve measured at $T = 300$ mK. (d) The "flipping-coin" experiment for a nanobrige. The plot displays the number of experiments (vertical axis) resulting in the given number of switchings (horizontal axis) for the constant testing current amplitude A indicated with a dashed vertical line for the S curve in (c). A single experiment consists of sending $N = 10\,000$ pulses and measuring the number of switchings. The experiment is repeated 35 372 times. The binomial distribution is superimposed as a black curve. ΔP_s is the statistical broadening of the measurement influencing the precision of the measured temperature.

switch to the normal state during the first few nanoseconds, its probability to switch at later times becomes exceedingly small owing to the exponential dependence of the switching rate on temperature (see Appendix B). As the cooling rate is reduced, the successive curves start to depart from the rest, with the $\tau_4 = 10$ ns curve separating first, the $\tau_4 = 50$ ns curve separating second, etc. Since the $\tau_4 = 10$ ns and $\tau_4 = 50$ ns relaxation curves are the same for the first approximately 70 ns, we conclude that in these first 70 ns, the temporal resolution is significantly better than 10 ns, with the switching happening predominantly at the beginning of the testing pulse. This proves that in the current experiment the temporal resolution is limited by the rise time of the arbitrary-waveform generator and not by the intrinsic response of the JJ thermometer.

V. STEADY-STATE TEMPERATURE PROFILE: MODELING

To obtain the temperature profile of the wire once the wire switches to the normal state, we solve the heat-balance equation in a steady state characterized by a constant electric current dissipating the Joule heat in the wire. The equation is

$$-\frac{d}{dx}\left(\kappa(T_e)\frac{dT_e}{dx}\right) = f(T_e), \qquad (2)$$

where left part of equation deals with hot-electron diffusion [$\kappa(T_e)$ is the electron thermal conductivity] and $f(T_e) = H(T_c)(ri_b^2)/S - \dot{q}_{ep}(T_e)$ is a source-drain term accounting for the power generation and absorption in a unit volume of the wire, where r is the resistance per unit length, S is the wire cross section, i_b is the biasing current, $H(T_c)$ is the Heaviside step function, and $\dot{q}_{ep}(T_e)$ is hot-electron power fed back to phonons. $\kappa(T_e)$ and $\dot{q}_{ep}(T_e)$ are numerical data calculated according to the integrals found in Refs. [33,34] (see Supplemental Material [32]). At $T_e > T_c$, $\dot{q}_{ep}(T_e)$ is equal to $\sum(T_e^5 - T_{ph}^5)$, with $\sum = 1.8 \times 10^9$ W/m^3 K^5 being the electron-phonon coupling constant in aluminum. The theoretical steady-state profile corresponding to our experimental realization is presented in the inset in Fig. 6(b). Since the profile is flat in the center of the wire, the only heat transfer under consideration
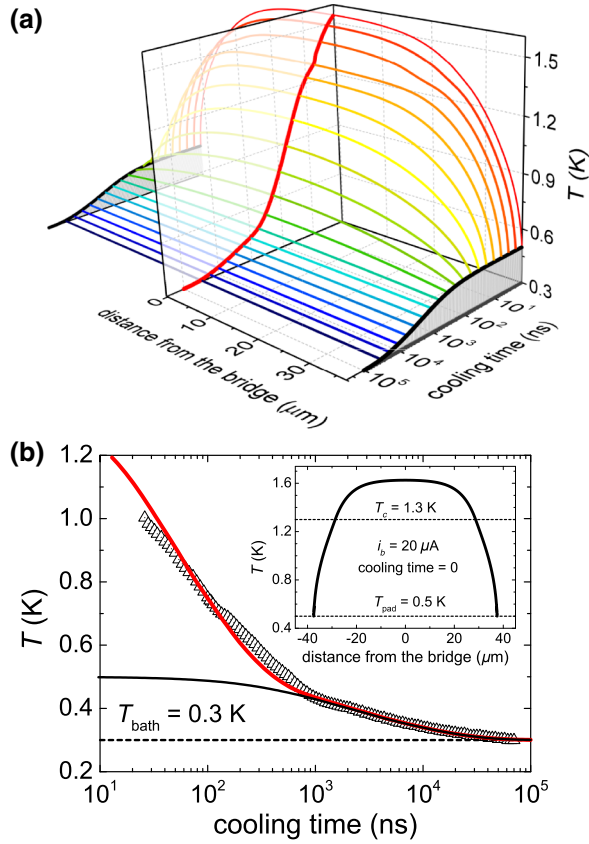
FIG. 6. Numerical modeling of temperature relaxation in the superconducting nanowire. (a) Temporal evolution of temperature profile in the wire. Temperature variations in the bridge and in the pads are distinguished with separate curves (red and black, respectively). (b) Modeled bridge (solid red curve) and pad (solid black curve) temperatures [the same as the curves distinguished in (a)] compared with experimental relaxation [black triangles, the same data as in Fig. 5(b)]. The cooling time $t = 0$ is set to be the end of the heating pulse bringing the wire to a steady state with $T \simeq 1.6$ K in the center of the wire (at the nanobridge location). The corresponding temperature profile is shown in the inset.

is heat flow from hot electrons to phonons ($f(T_e) = 0$), yielding for our experiment with $A_H = 20$ μA (see Fig. 3 and Supplemental Material [32]) an electron temperature of $T_e \simeq 1.6$ K in the center of the wire (at the nanobridge location).

VI. RELAXATION: MODELING

The cooling of the wire is governed by the temporal-relaxation equation taking into account two relaxation paths for the excess electron energy: the electron-phonon coupling and the diffusion of hot electrons:

$$\frac{d}{dx}\left(\kappa(T_e)\frac{dT_e}{dx}\right) = c_s(T_e)\frac{\delta T_e}{\delta t} + \dot{q}_{ep}(T_e), \qquad (3)$$

where $c_s(T_e)$ is the experimentally determined heat capacity of aluminum found in Ref. [35] (see Supplemental Material [32]). The initial condition is assumed to be the steady-state profile introduced above and displayed in the inset in Fig. 6(b) and the boundary conditions are dictated by the temperature of the pads. The calculated temperature relaxation in the superconducting wire and the measurement results are presented in Fig. 6. The fast relaxation within the first microsecond involves processes leading to equalization of the temperature in the whole wire with the temperature of the pads. More-detailed analysis (see Supplemental Material [32]) shows that above approximately 0.9 K, electron-phonon relaxation dominates, while below approximately 0.6 K, hot-electron diffusion takes over as electron-phonon relaxation becomes very inefficient. The slow relaxation reflects the dynamics of the electron-phonon heat transfer in the pads. Under the assumption that the pads are perfect energy reservoirs, the model is in qualitative agreement with the experimental relaxation profile during the first microsecond but it is not able to explain the long relaxation tail extending into the tens-of-microseconds range. Similar modeling for an initial temperature of the center of the wire of 3.3 K is presented in Supplemental Material [32]. It is important to note that a small adjustment of the heat capacity and electron-phonon coupling data may account for the observed difference between experimental points and theory. Since our primary goal is to demonstrate our proposed approach to thermometry and its temporal-resolution superiority, rather than to determine the detailed temperature dependence of the aluminum heat capacity, we calculate the temperature relaxation without any adjustment for the material parameters, solely on the basis of the data available from the literature. Our modeling does not take into account hot electrons fanning out from the nanowire ends toward massive contact pads. In principle, such two-dimensional diffusion effectively increases the nanowire length, but our wire is assumed to be sufficiently long to ignore this effect. Similarly we assume that the temperature of the pads is uniform at all stages of relaxation.

VII. DISCUSSION

We benchmark the ultrafast thermometry protocol using an aluminum Dayem nanobridge as a temperature-sensing element. However, the method will work for any kind of JJ that exhibits the dependence of switching current on temperature. Subject to the temperature interval of interest, one may use a tunnel junction or a proximity junction (e.g., a superconductor–normal-metal–superconductor junction). By selection of proper materials and adjustment of the length of the normal bridge (in the latter case), one can engineer an operational temperature range and magnitude of the switching current to match experimental requirements; for example, detection of

gigahertz photons or investigation of the thermal properties of quantum circuits may call for a titanium Dayem nanobridge, which is expected to work below 300 mK or a superconductor–normal-metal–superconductor proximity junction, with the greatest sensitivity near 100 mK [3]. On the other hand, use of niobium would allow one to perform switching thermometry at temperatures of around a few kelvins. The method is not only applicable to metallic circuits; it may also be used to explore heat flows through an electrically insulating silicon substrate with a heater and a JJ switching thermometer isolated electrically both on the top of the substrate. The wide range of available JJs makes our method universal and allows the testing of nanostructures based on different materials—superconductors, normal metals, semiconductors—involving experiments conducted in a magnetic field [27].

Temperature is an equilibrium concept, and its application to describe the state of a rapidly heated or cooling system may raise some questions. In solid-state physics, temperature determines the occupation of electron states (in equilibrium according to the Fermi-Dirac distribution). There are situations when the electron distribution is far from equilibrium, but without external excitation it locally quickly converges to the Fermi-Dirac function due to fast electron-electron interaction. It happens on timescales much shorter than the relaxation times considered in the experiment presented. We assume that the electron subsystem undergoes quasistatic evolution and is described locally at each moment by an equilibrium Fermi-Dirac distribution. Thus, the temperature of the electron system is well defined all the time during relaxation. Our concept of temperature measurement can be extended to probe nonequilibrium systems (i.e., where electrons are not Fermi-Dirac distributed). In such a case the measured temperature is called the "effective temperature" and corresponds to the equilibrium temperature if the same physical effect is observed (e.g., the same switching current).

Variations of the switching current in JJs are determined by two factors: (i) the value of the superconducting gap (it is a local property of the junction that sets the critical current) and (ii) the strength of electromagnetic fluctuations induced by the environment (it is a nonlocal property that may make the junction sensitive to temperature of remote electrical impedance, which is a source of the Johnson-Nyquist noise). In the case of a Dayem nanobridge with a critical current of about 100 μA, as the one studied here, the first factor dominates, and fluctuations play a minor role. However, for a tunnel junction with a low critical current, fluctuations will dominate and a sensor based on such a junction will be sensitive to a nonlocal temperature of the environment.

The thermometry presented is interesting with respect to power dissipation. The pulses probing a JJ thermometer have steep rising slopes and with standard equipment can be made shorter than 1 ns. Consequently, they cause

negligible heating of the sample and do not raise the sample temperature. This is in contrast to familiar dc and rf techniques where probing signals may alter the temperature that one wishes to measure.

VIII. OUTLOOK

JJ thermometers, located at various places on an electronic chip, will offer fast and high spatial resolution
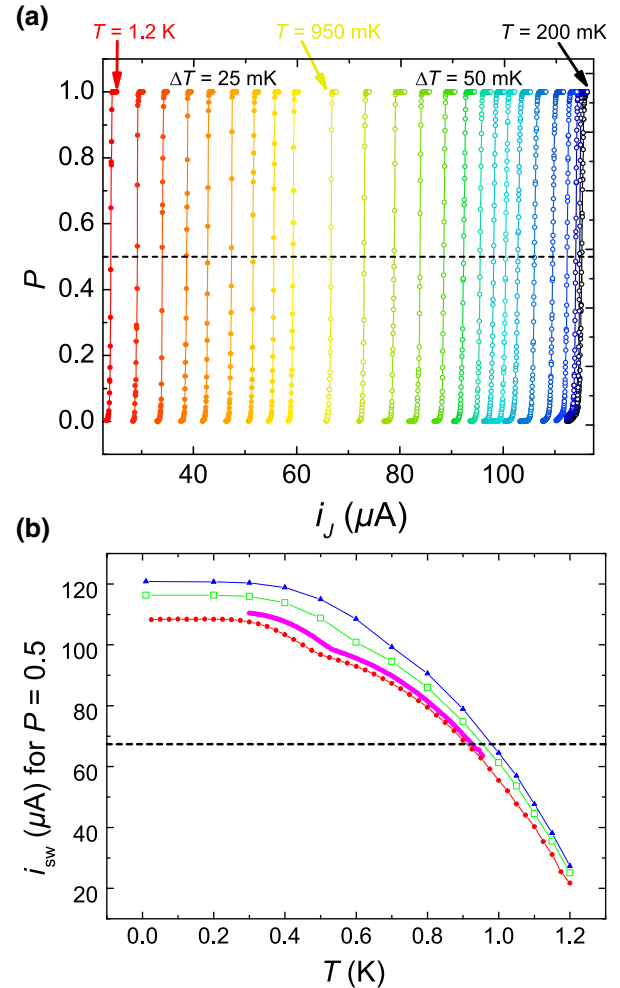

FIG. 7. (a) A typical collection of S curves measured at different temperatures used to extract the dependence of the switching current on temperature [i.e., the $i_{sw}(T)$ calibration curve]. The points are experimental data and the lines are guides for the eye. The dashed line corresponds to $P = 0.5$. (b) Temperature dependence of the switching current $i_{sw}(T)$ measured with different duration of the testing time τ_4 of the pump and probe pulses (from top to bottom): 10 ns, 50 ns, 200 ns, and 1 μs. The switching rate for each curve is 6.9×10^7, 1.4×10^7, 3.5×10^6, and 6.9×10^5 Hz, respectively. The dashed line is used to draw attention to the temperature variation of the switching rate Γ at a given current. This variation is important to understand switching dynamics in relaxation measurements when the temperature during the testing pulse is not constant (see Appendix B).

for mapping the temperature across the chip. They will allow one to analyze the effect of fast electrical pulses and photon absorption on the chip temperature distribution, thus helping to develop cryoelectronics, involving bolometers and quantum-computing devices. The unprecedented temporal resolution of the thermometer allows one to "see" heat propagating across different nanostructures (e.g., to observe hot-electron diffusion in real time and investigate mechanisms of heat dissipation via phonon- or photon-emission channels) [9]. The pump-and-probe protocol described is not compatible with detection of randomly arriving photons (e.g., in astrophysics they arrive with Poissonian temporal uncertainty). However, the proposed thermometer can be considered as a base sensing element for bolometers if photons are produced on demand in a well-defined time window (e.g., in cavity quantum electrodynamics using qubits or artificial atoms as photon sources). Owing to its very small size, the JJ-based thermometer could be integrated with a very small absorber with all three dimensions being a few tens of nanometers, providing a versatile platform for subattojoule-per-kelvin calorimetry. A small metal volume of 10^5–10^6 nm^3 used as the absorber yields a heat capacity of $(10^2$–$10^3)k_B$, offering high gains in sensitivity and temporal resolution of incident radiation [36]. Absorption of a single microwave photon (2–20 GHz) would produce a detectable 10-mK temperature spike, allowing one to count arriving photons and investigate the statistics of heat transport in superconducting quantum circuits. The temporal resolution of the thermometer can be shifted into the subnanosecond range with application of standard

gigahertz-limited arbitrary-waveform generators and sample design compatible with microwave propagation.

IX. CONCLUSION

We create a new paradigm of switching thermometry for nanoscale applications. Using the well-known technique of current pulses probing a Josephson junction, we show how the technique can be used for nanosecond-resolution temperature measurements. Superconducting weak links exhibit a very fast intrinsic dynamics (in the picosecond range) and are perfectly suited for sensing rapidly changing electron temperature, with subnanosecond temporal resolution easily achievable in the future. Our measurement gives insight into fast temperature relaxation of a superconducting nanowire, yielding an experimental estimate for the retrapping time. Successful implementation of our approach paves the way to cutting-edge experiments in the field of thermodynamics of low-temperature quantum circuits.
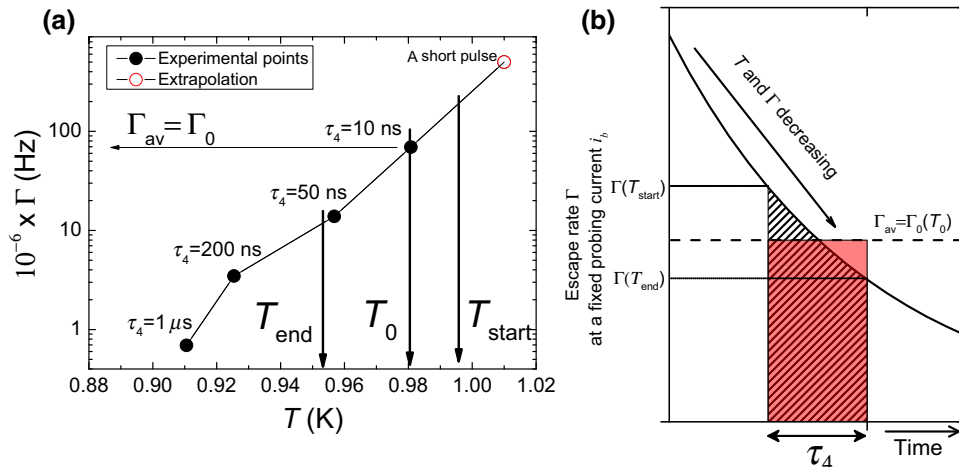
FIG. 8. (a) Experimental temperature dependence of the switching rate at a current of 67.4 μA extracted with aid of Fig. 7(b). T_{start} and T_{end} denote the temperature of the bridge at the beginning and at the end of the $\tau_4 = 10$ ns testing pulse, and are chosen here arbitrarily for the sake of demonstration. T_0 is an average temperature corresponding to an average rate $\Gamma_{\text{av}} = \Gamma_0$—the one if the bridge were measured at constant temperature T_0. (b) The temporal changes in the switching rate during a testing pulse of duration τ_4. Shaded areas are graphical representations of integrals: $\int_0^{\tau_4} \Gamma(t, i_b) dt$ and $\Gamma_{\text{av}}(T_0)\tau_4$.

research infrastructure for micro- and nanotechnologies (OtaNano).

APPENDIX A: $i_{SW}(T, P = 0.5)$ CALIBRATION CURVE EXTRACTED FROM S CURVES MEASURED AT DIFFERENT BATH TEMPERATURES

The set of S curves measured at different bath temperatures is presented in Fig. 7(a). The $i_{sw}(T)$ calibration curves for different durations of the testing time τ_4 are displayed in Fig. 7(b).

In general, the shape of the measured S curves reveals information about a fundamental mechanism governing the transition from the superconducting state to the normal state. The escape process is known to be driven either by thermal fluctuations or by quantum fluctuations. In the former case, the fitting of an Arrhenius-like relation to the experimental data allows one to independently determine the temperature of the electromagnetic environment. A higher fitted escape temperature can be an indication of macroscopic quantum tunneling or a multiphase slip-escape process. For the orthodox thermally driven escape, one observes a monotonic increase in the S-curve width when the temperature is increased. This is not what we observe for our nanobridge. Instead, we see a reduction of the width with increase of temperature, pointing to a mechanism other than the orthodox thermal mechanism underlying the switching. The simple calibration method used in our work is the most reliable way to interpret the switching current in terms of physical temperature.

APPENDIX B: CONVERSION OF THE SWITCHING CURRENT TO TEMPERATURE

To convert the switching current from the relaxation curves to the dynamic temperature, we use the $i_{sw}(T)$ calibration relationship. However, in our doing so, some care is needed. To obtain the calibration curve we measure switching currents at constant temperatures, whereas relaxation curves are acquired in a nonequilibrium condition: during the probing pulse the switching rate changes dramatically. The rate Γ corresponding to the switching probability for a pulse of duration τ, in equilibrium, verifies the equation $P = 1 - \exp[-\Gamma(T, i_b)\tau]$, where the electron-temperature T and biasing-current i_b dependence of the rate is displayed explicitly. The relation applied for different values of τ allows us to extract an experimental rate dependence on the temperature for a fixed value of i_b. Such a dependence for $i_b = 67.4 \, \mu A$ and $P = 0.5$ is shown in Fig. 8(a). When the junction is tested while its temperature decreases, the switching-probability determination must involve integration over rates experienced by the junction during the duration of the probing pulse τ_4; that is, in the time when the junction temperature drops
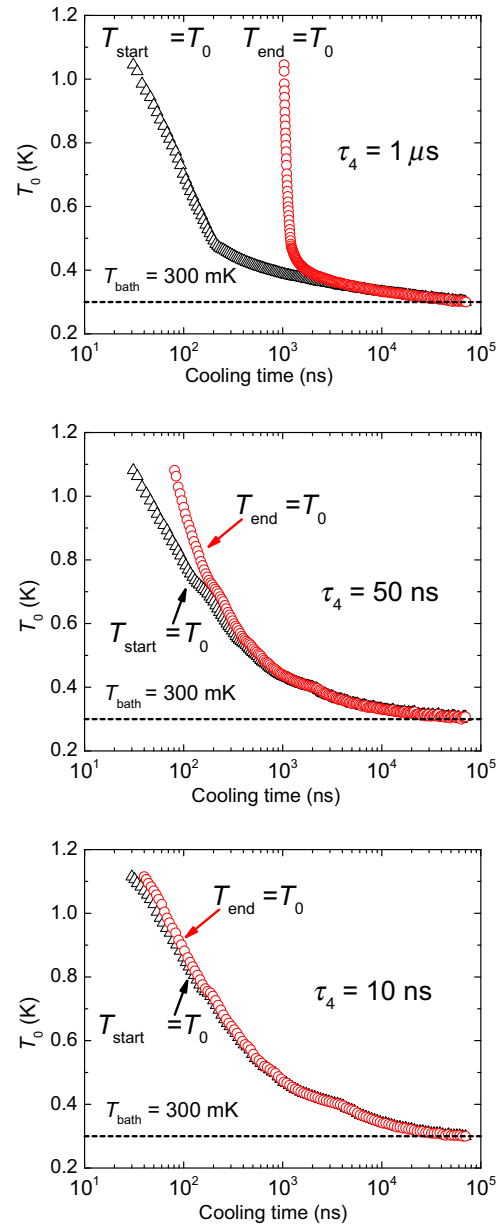

FIG. 9.   The effect of the testing pulse duration τ_4 on the temporal resolution of the determined temperature. Black triangles and red circles are plotted under the assumption that the temperature T_0 read from the $i_{sw}(T)$ calibration curve is the bridge temperature at the beginning of the testing pulse and at the end of the testing pulse, respectively. The bridge achieves temperature T_0 somewhere in time confined by the start and the end of the testing pulse. Resolution is limited by the "size of the probing tip."

from T_{start} to T_{end} [Fig. 8(b)]:

$$P = 1 - \exp\left[-\int_{0(T_{start})}^{\tau_4(T_{end})} \Gamma(t, i_b)dt\right]$$
$$= 1 - \exp[-\Gamma_{av}(i_b)\tau],$$

where $\Gamma_{av}(i_b)$ is the average switching rate during the relaxation process and is equal to $\Gamma_0(T_0, i_b)$ achieved in equilibrium for a known constant temperature, T_0, which can be read from the $i_{sw}(T)$ calibration curve (we define $i_{sw} = i_b$ for $P = 0.5$). Since $\Gamma(T_{start}) > \Gamma_{av} = \Gamma_0(T_0) > \Gamma(T_{end})$, we conclude that $T_{start} > T_0 > T_{end}$; that is, the junction reaches a well-specified temperature T_0 in the time interval confined by the duration of the current pulse. We define the two limits for the time in which the actual temperature T_0 is obtained: (i) T_0 is the temperature at the beginning of the current pulse; (ii) T_0 is the temperature at the end of the current pulse (Fig. 9). Such an approach imposes temporal uncertainty on the temperature determination equal to the pulse duration, but allows straightforward use of the $i_{sw}(T)$ calibration curve for conversion of the switching current to the dynamic temperature. The arbitrary-waveform generator used in our experiment produces the shortest pulses of about 10-ns duration but this duration can be reduced by at least 1 order of magnitude with more-advanced arbitrary-waveform generators available in the market. It is possible to develop a more-involved, switching-model-dependent scheme to convert the switching current into the dynamic temperature, but the treatment above has the advantage of being straightforward and leaves no room for speculation.

---

[1] S. Gasparinetti, K. L. Viisanen, O.-P. Saira, T. Faivre, M. Arzeo, M. Meschke, and J. P. Pekola, Fast Electron Thermometry for Ultrasensitive Calorimetric Detection, Phys. Rev. Appl. **3**, 014007 (2015).

[2] D. R. Schmidt, C. S. Yung, and A. N. Cleland, Temporal measurement of hot-electron relaxation in a phonon-cooled metal island, Phys. Rev. B **69**, 140301 (2004).

[3] O.-P. Saira, M. Zgirski, K. L. Viisanen, D. S. Golubev, and J. P. Pekola, Dispersive Thermometry with a Josephson Junction Coupled to a Resonator, Phys. Rev. Appl. **6**, 024005 (2016).

[4] A. V. Feshchenko, L. Casparis, I. M. Khaymovich, D. Maradan, O.-P. Saira, M. Palma, M. Meschke, J. P. Pekola, and D. M. Zumbühl, Tunnel-Junction Thermometry Down to Millikelvin Temperatures, Phys. Rev. Appl. **4**, 034001 (2015).

[5] J. Beyer, D. Drung, A. Kirste, J. Engert, A. Netsch, A. Fleischmann, and C. Enss, A magnetic-field-fluctuation thermometer for the mK range based on SQUID-magnetometry, IEEE Trans. Appl. Supercond. **17**, 760 (2007).

[6] S. Gasparinetti, F. Deon, G. Biasiol, L. Sorba, F. Beltram, and F. Giazotto, Probing the local temperature of a two-dimensional electron gas microdomain with a quantum dot: Measurement of electron-phonon interaction, Phys. Rev. B **83**, 201306 (2011).

[7] F. C. Wellstood, C. Urbina, and John Clarke, Hot-electron effects in metals, Phys. Rev. B **49**, 5942 (1994).

[8] K. Schwab, E. A. Henriksen, J. M. Worlock, and M. L. Roukes, Measurement of the quantum of thermal conductance, Nature **404**, 974 (2000).

[9] M. Meschke, W. Guichard, and J. P. Pekola, Single-mode heat conduction by photons, Nature **444**, 187 (2006).

[10] S. Jezouin, F. D. Parmentier, A. Anthore, U. Gennser, A. Cavanna, Y. Jin, and F. Pierre, Quantum limit of heat flow across a single electronic channel, Science **342**, 601 (2013).

[11] J. V. Koski, A. Kutvonen, I. M. Khaymovich, T. Ala-Nissila, and J. P. Pekola, On-Chip Maxwell'S Demon as an Information-Powered Refrigerator, Phys. Rev. Lett. **115**, 260602 (2015).

[12] M. Nahum, T. M. Eiles, and John M. Martinis, Electronic microrefrigerator based on a normal-insulator-superconductor tunnel junction, Appl. Phys. Lett. **65**, 3123 (1994).

[13] D. R. Schmidt, C. S. Yung, and A. N. Cleland, Nanoscale radio-frequency thermometry, Appl. Phys. Lett. **83**, 1002 (2003).

[14] Edouard Pinsolle, Alexandre Rousseau, Christian Lupien, and Bertrand Reulet, Direct Measurement of the Electron Energy Relaxation Dynamics in Metallic Wires, Phys. Rev. Lett. **116**, 236601 (2016).

[15] Anthony J. Fitzgerald, Vincent P. Wallace, Mercedes Jimenez-Linan, Lynda Bobrow, Richard J. Pye, Anand D. Purushotham, and Donald D. Arnone, Terahertz pulsed imaging of human breast tumors, Radiology **239**, 533 (2006).

[16] R. Appleby and H. B. Wallace, Standoff detection of weapons and contraband in the 100 GHz to 1 THz region, IEEE Trans. Antennas Propag. **55**, 2944 (2007).

[17] Bradley Ferguson and Xi-Cheng Zhang, Materials for terahertz science and technology, Nat. Mater. **1**, 26 (2002).

[18] Y.-F. Chen, D. Hover, S. Sendelbach, L. Maurer, S. T. Merkel, E. J. Pritchett, F. K. Wilhelm, and R. McDermott, Microwave Photon Counter based on Josephson Junctions, Phys. Rev. Lett. **107**, 217401 (2011).

[19] J. Govenius, R. E. Lake, K. Y. Tan, and M. Möttönen, Detection of Zeptojoule Microwave Pulses using Electrothermal Feedback in Proximity-Induced Josephson Junctions, Phys. Rev. Lett. **117**, 030802 (2016).

[20] Boris S. Karasik, Sergey V. Pereverzev, Alexander Soibel, Daniel F. Santavicca, Daniel E. Prober, David Olaya, and Michael E. Gershenson, Energy-resolved detection of single infrared photons with $\lambda = 8$ μm using a superconducting microbolometer, Appl. Phys. Lett. **101**, 052601 (2012).

[21] M. Zgirski, L. Bretheau, Q. Le Masne, H. Pothier, D. Esteve, and C. Urbina, Evidence for Long-Lived Quasiparticles Trapped in Superconducting Point Contacts, Phys. Rev. Lett. **106**, 257003 (2011).

[22] M. L. Della Rocca, M. Chauvin, B. Huard, H. Pothier, D. Esteve, and C. Urbina, Measurement of the Current-Phase Relation of Superconducting Atomic Contacts, Phys. Rev. Lett. **99**, 127005 (2007).

[23] Marek Foltyn and Maciej Zgirski, Gambling with Superconducting Fluctuations, Phys. Rev. Appl. **4**, 024002 (2015).

[24] I. Chiorescu, Y. Nakamura, C. J. P. M. Harmans, and J. E. Mooij, Coherent quantum dynamics of a superconducting flux qubit, Science **299**, 1869 (2003).

[25] John M. Martinis, Michel H. Devoret, and John Clarke, Experimental tests for the quantum behavior of a macroscopic degree of freedom: The phase difference across a Josephson junction, Phys. Rev. B **35,** 4682 (1987).

[26] M. Devoret, D. Esteve, C. Urbina, J. Martinis, A. Cleland, and J. Clark, in *Exploring the Quantum Classical Frontier: Recent Advances in Macroscopic Quantum Phenomena,* editor by J. Friedman and S. Han (Nova Science Publishers, New York, 2003).

[27] W. Wernsdorfer, From micro-to nano-squids: Applications to nanomagnetism, Superconductor Science and Technology **22,** 064013 (2009).

[28] Francesco Giazotto, Tero T. Heikkilä, Arttu Luukanen, Alexander M. Savin, and Jukka P. Pekola, Opportunities for mesoscopics in thermometry and refrigeration: Physics and applications, Rev. Mod. Phys. **78,** 217 (2006).

[29] C. W. J. Beenakker, Universal Limit of Critical-Current Fluctuations in Mesoscopic Josephson Junctions, Phys. Rev. Lett. **67,** 3836 (1991).

[30] Vinay Ambegaokar and Alexis Baratoff, Tunneling between Superconductors, Phys. Rev. Lett. **10,** 486 (1963).

[31] M. Tinkham, *Introduction to Superconductivity,* Dover Books on Physics (Dover Publications, Mineola, New York, 2004), 2nd ed.

[32] See Supplemental Material at http://link.aps.org/supplemental/10.1103/PhysRevApplied.10.044068 for the graphical conversion of the switching current to temperature and extended modeling along with the numerical parameters used for the simulations.

[33] H. Courtois, M. Meschke, J. T. Peltonen, and J. P. Pekola, Origin of Hysteresis in a Proximity Josephson Junction, Phys. Rev. Lett. **101,** 067002 (2008).

[34] V. F. Maisi, S. V. Lotkhov, A. Kemppinen, A. Heimes, J. T. Muhonen, and J. P. Pekola, Excitation of Single Quasiparticles in a Small Superconducting Al Island Connected to Normal-Metal Leads by Tunnel Junctions, Phys. Rev. Lett. **111,** 147001 (2013).

[35] Norman E. Phillips, Heat capacity of aluminum between 0.1 and 4.0 K, Phys. Rev. **114,** 676 (1959).

[36] $\Delta T = Q/C$, the temperature rise of the absorber ΔT on absorption of a small amount of energy Q, is inversely proportional to the heat capacity of the absorber C (high sensitivity); $\tau = C/G$, the relaxation time of the absorber, is proportional to its heat capacity C, with G being heat conductance (fast response).